Micromechanical characterization of the interphase layer in semi-crystalline polyethylene

Akbar Ghazavizadeh*[a,b], Gregory C. Rutledge[c], Ali A. Atai[b], Saïd Ahzi[a,d], Yves Rémond[a], Nasser Soltani[b]

[a]Université de Strasbourg-CNRS, ICube, 2 rue Boussingault, 67000 Strasbourg, France
[b]School of Mechanical Engineering, University College of Engineering, University of Tehran, P.O. Box 11365-4563 Tehran, IRAN
[c]Department of Chemical Engineering, Massachusetts Institute of Technology, 77 Massachusetts Avenue, Cambridge, MA 02139, USA
[d]School of Materials Science and Engineering, Georgia Institute of Technology, Atlanta, GA 30332, USA

ABSTRACT

Semi-crystalline polyethylene is composed of three domains: crystalline lamellae, the compliant amorphous phase, and the so-called "interphase" layer separating them. Among these three constituents, little is known about the mechanical properties of the interphase layer. This lack of knowledge is chiefly due to its mechanical instability as well as its nanometric thickness impeding any property measuring experiments. In this study, the Monte Carlo molecular simulation results for the interlamellar domain (i.e. amorphous+ interphases), reported in (in 't Veld et al. 2006) are employed. The amorphous elastic properties are adopted from the literature and then two distinct micromechanical homogenization approaches are utilized to dissociate the interphase stiffness from that of the interlamellar region. The results of the two approaches match perfectly, which validates the implemented dissociation methodology. Moreover, a hybrid numerical technique is proposed for one of the approaches when the recursive method poses numerical divergence problems. Interestingly, it is found that the dissociated interphase stiffness lacks the common feature of positive definiteness, which is attributed to its nature as a transitional domain between two coexisting phases. The sensitivity analyses carried out reveal that this property is insensitive to the non-orthotropic components of the interlamellar stiffness as well as the uncertainties existing in the interlamellar and amorphous stiffnesses. Finally, using the dissociated interphase stiffness, its effective Young's modulus is calculated. The evaluated Young's modulus compares well with the effective interlamellar Young's modulus for highly crystalline polyethylene, reported in an experimental study. This satisfactory agreement along with the identical results produced by the two micromechanical approaches confirms the validity of the new information about the interphase elastic properties in addition to making the proposed dissociation methodology quite reliable to be applied to similar problems.

Keywords: semi-crystalline polyethylene; interphase layer; micromechanical homogenization, sensitivity analysis.

1. Introduction

Semi-crystalline polyethylene (PE) of different grades is reputed to be the most widely used/produced plastic worldwide. Its widespread use is due to excellent resistance to chemical agents and physical shocks as well as reasonable mechanical properties at ambient temperature and at an economic price. Its mechanical performance is due primarily to its microscale composite structure. Microstructurally, PE is composed of two major components: crystalline lamellae, also known as crystallites, and the amorphous interlamellar phase, also known as the noncrystalline phase.

Upon crystallization from melt, the regular arrangement of chains in an orthorhombic crystalline system [1,2] forms the crystalline lamellae whose radial array, in turn, contributes to the spherulitic morphology of PE in a larger scale [3,4]. The mechanical properties of the crystalline phase have been well

established during the recent decades [5-10]. On the other hand, the noncrystalline, interlamellar phase entrapped between the crystallites has no predefined structure. Therefore, researchers used to name this interlamellar phase as "amorphous phase" hence describing PE as a two-phase composite. However, the sharp transition from crystalline to amorphous state is hypothetically impossible. By relying on experimental observations and theoretical arguments [11-13] a broad consensus has been created among researchers that the non-crystalline domain itself can be viewed as a two-component sandwich: a central, compliant, amorphous core with two more rigid, amorphous layers at the sides. Accordingly, the two composing phases of the non-crystalline interlamellar region are amorphous in structure but the central phase is less rigid than the side/intermediate layers. In the literature the former is referred to as the amorphous phase and the latter as the "interphase". The term "interphase" was first employed by Flory [14] to define an interfacial zone between two immiscible phases. The term "rigid amorphous phase" has also been used to describe a noncrystalline component that remains immobilized even above the glass transition point of the polymer, possibly as a consequence of proximity to the crystalline lamellae [13]. A schematic diagram of the composing phases of PE is illustrated in Fig. 1. The recognition of the interphase is due in large part to the stronger anchorage to the adjacent crystallite rendering this separating layer stiffer than the central amorphous phase, which is rather liquid-like at temperatures above T_g. Therefore, in three-component micromechanical modeling of PE, the mechanical properties of this less-known third component are requisite.

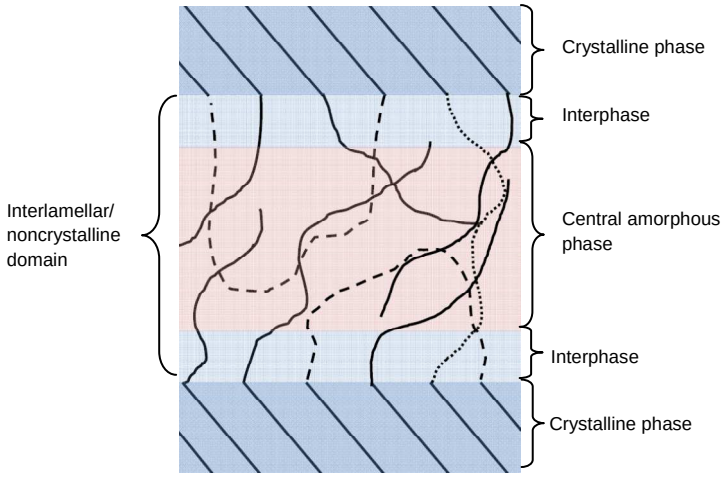

Fig. 1 Schematic diagram of the crystalline and noncrystalline (interphase + amorphous) domains in PE

In their three-component micromechanical modeling of PE, Sedighiamiri et. al. [15] took the interphase layer to be isotropic whereas its true symmetry, as will be discussed next, is monoclinic. Additionally, they chose an average interphase bulk modulus, κ_{ip}, of 5000 MPa, which is an intermediate value between the crystalline and amorphous bulk moduli, and left the average interphase shear modulus, G_{ip}, as the fitting parameter. In a similar study on the three-phase micromechanical modeling of PET, Gueguen et. al. [16] took the associated interphase stiffness to be 1.6 times that of the amorphous phase, i.e $\mathcal{C}^{ip} = 1.6\mathcal{C}^{am}$. They assert that by this specific selection, some "best fit" is observed, which indicates that they have treated the coefficient as an adjustable parameter. In similar studies concerning filler/polymer composites where some intermediate or interphase layer around the fillers is incorporated into the modeling, the properties of this third phase have been treated alike [17-19]. Although several studies have been devoted to the mechanical characterization of the central amorphous phase, to date no rigorous attention has been paid to the systematic, methodological elastic characterization of the interphase as is presented in this work. At the molecular simulation level, Hütter et. al. [1] employed the concept of a sharp Gibbs dividing surface in order to define a set of interfacial properties corresponding to the interphase; they obtained interfacial stresses and interfacial internal energies, but were not able to

extract a value for interfacial tension due to significant contributions from its dependence on interfacial strain.

Here, two independent micromechanical homogenization approaches are tailored to extract the interphase stiffness from that of the interlamellar domain. Then they are applied to the Monte Carlo (MC) molecular simulation results by in 't Veld et. al [20] who reported the variation of the interlamellar stiffness components, $\mathcal{C}_{ij}^{il}$, with temperature for the range of 350-450 K. First, the findings and observations of different pertinent theoretical and experimental investigations are exploited to establish a plausible temperature-dependent amorphous stiffness. Then, the two known stiffnesses, i.e. $\mathcal{C}^{il}$ and $\mathcal{C}^{am}$, along with their associated thicknesses [20], are fed into the dissociation algorithms. Due to the absence of experimental measurements on the mechanical properties of the interphase, which have remained elusive as yet, direct verification of the calculated interphase stiffness components is not possible. Nonetheless, we could successfully compare the average effective Young's modulus of the dissociated interphase with the available experimental results on the average interlamellar Young's modulus at high crystallinity [21]. In the present study, two agreements are observed which corroborate the validity of the results as well as the efficiency of the presented methodology: Firstly, an excellent agreement is observed between the results of the two deployed micromechanical homogenization techniques whose origins are totally different; Secondly, a good agreement is observed between the interphase average Young's modulus, which is evaluated using the results of this study, and the interlamellar average Young's modulus at high crystallinity, which is offered in the experimental study by Crist et al. [21].

The following sections are organized as follows: Section 2 details the reasoning behind the adopted amorphous elastic constants and then introduces the two micromechanical approaches, which are tailored for the dissociation purpose. Section 3 is devoted to discussing the results and diagrams of the dissociated interphase stiffness, including Subsection 3.3 where the results are verified by comparing with the observations of another experimental study. A concise summary along with the conclusions drawn are brought in Section 4. To enhance the readability of the paper, the analytical details of one of the micromechanical models are moved to Appendix A. Appendix B is devoted to the details of the sensitivity analyses that were carried out to examine the robustness of the non-positive definiteness of the interphase stiffness to the uncertainties of the amorphous and interlamellar stiffnesses, and the impact of the small components of the interlamellar and interphase stiffnesses on one another.

2. Methodology

As illustrated in Fig. 1, the interlamellar domain in PE consists of an amorphous phase surrounded by two interphase layers. The elastic stiffness of this interlamellar domain, $\mathcal{C}^{il}$, is a function of the amorphous and interphase elastic stiffnesses, $\mathcal{C}^{am}$ and $\mathcal{C}^{ip}$, as well as their respective volume fractions, η_{am} and η_{ip}. As dissociating tools, two distinct analytical, micromechanical homogenization techniques, namely the double-inclusion method (DIM) and the extended composite inclusion model (ECIM), are applied in reverse mode to the MC molecular simulations of in 't Veld et al. [20] for the elastic characterization of the interphase layer. The components of $\mathcal{C}^{il}$ together with amorphous and interphase thicknesses, from which η_{am} and η_{ip} are calculable, are already available from MC molecular simulations for the temperature range of 350-450 K. Here, the simulation results up to 400 K, which is close to the melting point of bulk PE, i.e. 407 K, are taken advantage of.

If the final homogenization formulae for the interlamellar effective stiffness, which are obtained from the micromechanical homogenization techniques, are viewed as equations with the following general functional form:

$$F\left(\mathcal{C}^{\mathrm{il}},\mathcal{C}^{\mathrm{am}},\mathcal{C}^{\mathrm{ip}},\eta_{\mathrm{am}},\eta_{\mathrm{ip}}\right)=0 \tag{1}$$

then there is one equation from which only one unknown can be determined. In most homogenization problems encountered in the literature, the homogenization relations are utilized in direct mode to find the effective properties of some inhomogeneous medium using the properties and concentrations of the composing phases. Here, two of such homogenization techniques are employed in the reverse mode to find the unknown property of one of the constituents. But for the problem at hand, there are two unknowns: $\mathcal{C}^{\mathrm{am}}$ and $\mathcal{C}^{\mathrm{ip}}$. As to $\mathcal{C}^{\mathrm{am}}$, no suitable value is currently available from molecular simulations. Therefore, in the following subsection, first various relevant studies are surveyed to find an estimate for the amorphous elastic constants at room temperature using which $\mathcal{C}^{\mathrm{am}}$ is established and consequently $\mathcal{C}^{\mathrm{ip}}$ will be the only remaining unknown.

2.1. Amorphous elastic constants

The elastic constants of the amorphous PE have been the subject of research for decades [21-24]. Since obtaining fully amorphous PE samples at relevant temperatures is nearly impossible, the reported elastic values are either based on theoretical arguments or extrapolation to zero crystallinity of measurements made at non-zero crystallinities. Using the theoretical relationship for the plateau shear modulus

$$G_{\mathrm{N}}^{0}=\frac{\rho RT}{M_{\mathrm{e}}} \tag{2}$$

and an amorphous bulk modulus of $\kappa_{\mathrm{am}}=3000\,\mathrm{MPa}$, Bédoui et. al. [25] and Sedighiamiri et. al. [15] estimated the amorphous Young's modulus and Poisson's ratio to be $E_{\mathrm{am}}=4.5\,\mathrm{MPa}$ and $\upsilon_{\mathrm{am}}=0.49975$, respectively. In Eq.(2) ρ is the amorphous phase density, T the absolute temperature, R the ideal gas constant, and M_{e} the molecular mass between entanglements. Krigas et. al. [22] conducted several tests on different PE samples at different crosshead speeds (≤ 0.1 in/min) and observed that their curve-fit of PE Young's modulus and the one estimated from the rubbery plateau modulus intersect at a crystallinity of $\xi=0.03$. From the intercepts of the two graphs, they concluded that at room temperature $E_{\mathrm{am}}=3.5\pm0.5\,\mathrm{MPa}$. Hellwege et. al. [23] reported that at room temperature $\kappa_{\mathrm{am}}=1800\,\mathrm{MPa}$, where in combination with the results of Krigas et. al. [22] there obtains $\upsilon_{\mathrm{am}}\sim 0.4994$. Using the same technique of extrapolation to zero crystallinity, Crist et. al. [21] reported a value of $E_{\mathrm{am}}=2\,\mathrm{MPa}$. Again by extrapolation from melt properties at room temperature, Fetters et. al. [26] reported $G_{\mathrm{am}}=3.8\,\mathrm{MPa}$ from which the corresponding elastic modulus is slightly less than $3G_{\mathrm{am}}$, meaning that $E_{\mathrm{am}}\simeq 11.4\,\mathrm{MPa}$. Finally, Janzen [24] estimated $E_{\mathrm{am}}=4.1\,\mathrm{MPa}$ and $\upsilon_{\mathrm{am}}=0.4998$ after running quite a few tests on different PE samples.

Obviously, there is a fairly good agreement between different studies on the elastic properties of the amorphous phase at room temperature. The average of the above Poisson's ratios is ~ 0.4996 which is very close to the limit value of 0.5. The proximity of υ_{am} to 0.5 is due to the rubbery state of the amorphous phase at room temperature and *a fortiori* at higher temperatures. Therefore, it is totally reasonable to assume that υ_{am} remains nearly constant for the temperature range of interest with possibly negligible fluctuations around its mean value. For E_{am}, the average of the values reported in the previous studies for room temperature is ~ 5 MPa, which matches the mean value adopted by Humbert et al. [27] for the amorphous phase of polyethylene at room temperature. According to Eq.(2), which has been

introduced in the context of the kinetic theory of rubber elasticity, the elastic modulus of the amorphous phase is a linear function of temperature in the rubbery region. Moreover, using the first and second laws of thermodynamics and based on the probabilistic discussions, it is demonstrated that the elastic modulus of a single chain in an amorphous polymer in the rubbery state is proportional to

$$\frac{3kT}{nl^2} \tag{3}$$

where k is the Boltzmann constant and n is the number of links in the chain each having an average length l [28]. It is therefore quite justifiable to assume that E_{am} is a linear function of temperature across the temperature range of interest where the amorphous phase of PE is rubbery [29]. Accordingly, the following linear function is adopted for the temperature dependence of E_{am} for $350\,\text{K} \le T \le 400\,\text{K}$

$$E_{\text{am}} = 5\frac{T}{293}\left(\text{MPa}\right) \tag{4}$$

But it should be noted that E_{am} is a weak function of temperature (for instance $E_{\text{am}}\left(400\,\text{K}\right) = 6.8\,\text{MPa}$) and one may take E_{am} to remain almost constant for the entire rubbery zone; this assumption would be consistent with the diagrams of the storage modulus vs. temperature for typical amorphous polymers in the rubbery regime. Additionally, the two adopted amorphous elastic constants, namely υ_{am} and E_{am}, do not exhibit substantial changes within the considered temperature range to demand more precise estimations. Nevertheless, as demonstrated in Appendix B, using an *ad hoc* sensitivity analysis the impact of the possible uncertainties available in the adopted amorphous elastic constants on the generality of conclusions is evaluated. Based on careful examinations carried out, we believe that the basic conclusions remain essentially unaltered if more accurate forms of temperature dependence for υ_{am} and E_{am} were available. At any rate, the proposed methodology and dissociating tools presented herein remain applicable even if other forms of dependence are employed.

2.2. Micromechanical homogenization approaches of DIM and ECIM

Two distinct micromechanical homogenization techniques of DIM and ECIM are invoked to dissociate the interphase stiffness from that of the interlamellar domain. Although the primary function of multiscale homogenization methods is to calculate the effective properties of nonhomogeneous media, here two of such methods are reversely employed to find the elastic stiffness of one of the constituents in a two-phase heterogeneous medium.

Developed by Hori and Nemat Nasser [30], DIM proposes an Eshelby-based formulation for evaluating the homogenized stiffness of an ellipsoidal inclusion encapsulating another ellipsoid with the entire double-inclusion being embedded in a reference medium. In the MC molecular simulations, the periodic boundary conditions are imposed in a way that the interlamellar region can be treated as an inner, thin, disk-like ellipsoid, namely the core amorphous phase, wrapped by another hollow, thin, disk-like ellipsoid, namely the side interphase layers. Therefore, the problem under discussion fits the double-inclusion model if the Eshelby tensor of disk-like ellipsoids (i.e. an ellipsoid with a very small aspect ratio) is used. After some mathematical manipulation, the DIM relationship for the interphase stiffness is rendered into

$$\mathcal{C}^{\text{ip}} = \mathcal{C}^{\text{ref}} - \mathcal{C}^{\text{ref}}\left\{\left[\frac{1}{\eta_{\text{ip}}}\left[\left(\mathcal{I} - \left(\mathcal{C}^{\text{ref}}\right)^{-1}\mathcal{C}^{\text{il}}\right)^{-1} - \mathcal{S}^{\infty}\right]^{-1} - \frac{\eta_{\text{am}}}{\eta_{\text{ip}}}\left[\left(\mathcal{I} - \left(\mathcal{C}^{\text{ref}}\right)^{-1}\mathcal{C}^{\text{am}}\right)^{-1} - \mathcal{S}^{\infty}\right]^{-1}\right]^{-1} + \mathcal{S}^{\infty}\right\}^{-1} \tag{5}$$

Here, $\mathcal{I}$ represents the fourth order identity tensor and $\mathcal{S}^{\infty}$ stands for the Eshelby tensor of a disk-like inclusion inserted in a reference medium whose stiffness is $\mathcal{C}^{\text{ref}}$. The details of the assumptions and derivation of DIM formulations are available in the work of Hori and Nemat-Nasser [30].

Formulated first by Ahzi et. al. [31,32], the composite inclusion model (CIM) is an attempt to find a compromise between the Voigt and Reuss mixture formulae for a layered composite inclusion by introducing strain and stress concentration tensors which serve also as weight functions. In this approach, the composite inclusion is made by stacking together two layers whose thicknesses are much less than two other dimensions. The weight functions are established through the simultaneous enforcement of the continuity of deformation and equilibrium at the interface of the two composing layers. Here, the idea is extended to a three-layer composite inclusion, hence the designation extended composite inclusion model (ECIM). Again, owing to the nature of the periodic boundary conditions imposed in molecular simulations, the interlamellar region can be thought of as two thin interphase layers with one thin amorphous layer inserted in between. With reference to the notation defined in Appendix A, the dissociative analogue of Eq.(1) yielding the unknown $\mathcal{C}^{\text{ip}}$ is given by either of the following two equivalent equations:

$$\begin{aligned} \mathcal{C}^{\text{ip}} &= (1-\eta_{\text{am}})\,\mathcal{R}^{\text{ip}}\left[\left(\mathcal{C}^{\text{il}}\right)^{-1} - \eta_{\text{am}}\left(\mathcal{C}^{\text{am}}\right)^{-1}\mathcal{R}^{\text{am}}\right]^{-1} \quad \text{or} \\ \mathcal{C}^{\text{ip}} &= \left[\mathcal{C}^{\text{il}} - \eta_{\text{am}}\mathcal{C}^{\text{am}}\mathcal{Q}^{\text{am}}\right]\left((1-\eta_{\text{am}})\mathcal{Q}^{\text{ip}}\right)^{-1} \end{aligned} \tag{6}$$

where $\mathcal{R}^{\text{ip}}$, $\mathcal{R}^{\text{am}}$, $\mathcal{Q}^{\text{ip}}$ and $\mathcal{Q}^{\text{am}}$ are certain weight coefficients which are functions of η_{am}, $\mathcal{C}^{\text{ip}}$ and $\mathcal{C}^{\text{am}}$. For further details on the derivation of the ECIM relationships, see Appendix A.

As compared to DIM, the distinguishing feature of ECIM is that in its formulation, there is no trace of the Eshelby tensor, Green's function, the concept of reference medium or triple volume integrations, all being the indispensable elements to DIM derivation. One strength of the presented methodology lies in the perfect agreement between the solutions of the two approaches of DIM and ECIM, despite the fact that their origins are totally different.

Furthermore, a quick comparison between the DIM and ECIM relationships reveals that in DIM relation there appear $\mathcal{S}^{\infty}$ and $\mathcal{C}^{\text{ref}}$ in addition to the other independent variables appearing in ECIM relations. It is reminded that $\mathcal{S}^{\infty}$ is a function of $\mathcal{C}^{\text{ref}}$ as well as the aspect ratios (or geometry) of the ellipsoidal inclusion. Apart from the geometry of the problem, which has been taken into account during the derivation of the ECIM formulae, there's no need to resort to the concept of some "reference medium" in the ECIM. It is, therefore, anticipated that for this specific case where the ellipsoidal inclusion is disk-like, the DIM results will be independent of the choice of $\mathcal{C}^{\text{ref}}$. Although it looks too difficult to demonstrate it mathematically due to the nonlinear dependence of $\mathcal{S}^{\infty}$ on $\mathcal{C}^{\text{ref}}$ in addition to the nonlinear dependence of $\mathcal{C}^{\text{ip}}$ on both $\mathcal{S}^{\infty}$ and $\mathcal{C}^{\text{ref}}$, it seems to be a true conjecture. Strictly speaking, a large number of different $\mathcal{C}^{\text{ref}}$ s were picked as input for Eq.(5) and it was observed that the dissociated $\mathcal{C}^{\text{ip}}$ s are exactly identical indicating the independence of the dissociated $\mathcal{C}^{\text{ip}}$ from $\mathcal{C}^{\text{ref}}$.

3. Results and discussion

As suggested by in 't Veld et. al. [20] the interlamellar stiffness obtained from MC simulations has the following form of monoclinic symmetry

$$\mathcal{C}^{\mathrm{il}} = \begin{bmatrix} C_{11}^{\mathrm{il}} & C_{12}^{\mathrm{il}} & C_{13}^{\mathrm{il}} & 0 & -180 & 0 \\ C_{12}^{\mathrm{il}} & C_{22}^{\mathrm{il}} & C_{23}^{\mathrm{il}} & 0 & -240 & 0 \\ C_{13}^{\mathrm{il}} & C_{23}^{\mathrm{il}} & C_{33}^{\mathrm{il}} & 0 & 50 & 0 \\ 0 & 0 & 0 & 0 \pm 100 & 0 & -200 \\ -180 & -240 & 50 & 0 & 220 \pm 60 & 0 \\ 0 & 0 & 0 & -200 & 0 & 570 \pm 60 \end{bmatrix} \mathrm{MPa} \tag{7}$$

The numerical values of the non-tensile elements, i.e. the elements of $\mathcal{C}^{\mathrm{il}}$ other than the upper left 3×3 submatrix, were reported by in 't Veld et. al. [20] only at 435 K and are taken here to be virtually temperature independent, for lack of any better information. These values are provided explicitly in Eq.(7). It should be noted that the uncertainties associated with the shearing stiffnesses, which are reported on the right side of the mean values, are the result of MC simulations. On the contrary, the values of the tensile elements of $\mathcal{C}^{\mathrm{il}}$ were calculated over a range of temperature and this temperature dependency is adopted here as well; for this reason, the temperature-dependent tensile elements of $\mathcal{C}^{\mathrm{il}}$ are represented symbolically in Eq.(7). The reported uncertainty of these tensile components is $\pm 30\,\mathrm{MPa}$.

The output of the dissociation approaches, i.e. DIM and ECIM, at the typical temperature of 370 K is given in Table 1. As explained in the previous section, the DIM involves the Eshelby tensor for a disk-shaped inclusion, which must be evaluated numerically since it has no closed-form solution in the general case where the reference medium is anisotropic. Therefore, in the developed numerical code, a very small aspect ratio of $\mu \ll 1$ has been assumed for the calculation of the Eshelby tensor. It was also observed that due to the recursive nature of the ECIM in the dissociation mode (see Appendix A), the method has shown numerical divergence despite deploying several stabilizing strategies. Therefore, the following numerical alternative was invoked. First, $\mathcal{C}^{\mathrm{il}}$ was symbolically calculated by ECIM relations and using an unknown $\mathcal{C}^{\mathrm{ip}}$. A system of 13 coupled equations with 13 unknowns is thus obtained for the solution of which a hybrid optimization algorithm has been employed. The two-step, hybrid optimization algorithm consisted of combining the Genetic Algorithm with another non-linear optimization technique called Nelder-Mead (or simplex search) method. In the first step, a ballpark estimate for the solution is found using the Genetic Algorithm which is used as the initial guess for the Nelder-Mead method in the second step. The dissociated $\mathcal{C}^{\mathrm{ip}}$ attributed to ECIM in Table 1 is the result of this combinatory numerical method.

A quick comparison reveals that the results of the two methods agree perfectly. From a practical point of view, however, the ECIM formulation is fairly straightforward and simpler than the DIM formulation but is less efficient in the dissociation mode in terms of CPU time. Interestingly, and as discussed in Appendix B, when the non-orthotropic elements of the interlamellar stiffness are neglected, the combination of the dual ECIM formulae (6) converges to the solution using the recursive method, which is much faster than the hybrid optimization technique. In contrast, the DIM is very fast in both of the dissociation and homogenization modes but maybe its major drawback is the development of the rather complicated numerical code for calculating the Eshelby tensor.

In the direct/homogenization mode, however, when the dissociated $\mathcal{C}^{\mathrm{ip}}$ is used in combination with $\mathcal{C}^{\mathrm{am}}$ to produce the initial $\mathcal{C}^{\mathrm{il}}$, the ECIM and the DIM produce the correct solution quite fast. In view of the details provided in Appendix A, the ECIM formulation in the homogenization mode takes the following explicit form

$$\begin{aligned} &\mathcal{C}^{\mathrm{il}} = \left(1-\eta_{\mathrm{am}}\right)\mathcal{C}^{\mathrm{ip}}\mathcal{Q}^{\mathrm{ip}} + \eta_{\mathrm{am}}\mathcal{C}^{\mathrm{am}}\mathcal{Q}^{\mathrm{am}} \quad \text{or} \\ &\left(\mathcal{C}^{\mathrm{il}}\right)^{-1} = \left(1-\eta_{\mathrm{am}}\right)\left(\mathcal{C}^{\mathrm{ip}}\right)^{-1}\mathcal{R}^{\mathrm{ip}} + \eta_{\mathrm{am}}\left(\mathcal{C}^{\mathrm{am}}\right)^{-1}\mathcal{R}^{\mathrm{am}} \end{aligned} \tag{8}$$

Table 1: Output of dissociation approaches at the typical temperature of 370 K.

at T=370 K: $E_{am}=6.31\,\text{MPa}$, $G_{am}=2.10\,\text{MPa}$, $\eta_{am}=0.66$, $\eta_{ip}=0.34$												
$\mathcal{C}^{am}\,(\text{MPa})$							$\mathcal{C}^{il}\,(\text{MPa})$ (taken from [20])					
3097.9	3093.7	3093.7	0	0	0		1749.9	1613.6	1092.9	0	-180	0
3093.7	3097.9	3093.7	0	0	0		1613.6	2569.3	1150	0	-240	0
3093.7	3093.7	3097.9	0	0	0		1092.9	1150	1249.6	0	50	0
0	0	0	2.1	0	0		0	0	0	90*	0	-200
0	0	0	0	2.1	0		-180	-240	50	0	220	0
0	0	0	0	0	2.1		0	0	0	-200	0	570
Then:												
$\mathcal{C}^{ip}\,(\text{MPa})$ output by the DIM							1972.2	1307.4	427.7	0	3.05	0
							1307.4	3824.3	524.2	0	3.92	0
							427.7	524.2	567.3	0	-0.33	0
							0	0	0	**-1.11**	0	7.31
							3.05	3.92	-0.33	0	**-1.08**	0
							0	0	0	7.31	0	320.5
$\mathcal{C}^{ip}\,(\text{MPa})$ output by the ECIM (using the hybrid optimization algorithm)							1972.2	1307.4	427.7	0	3.05	0
							1307.4	3824.3	524.2	0	3.92	0
							427.7	524.2	567.3	0	-0.33	0
							0	0	0	**-1.11**	0	7.31
							3.05	3.92	-0.33	0	**-1.08**	0
							0	0	0	7.31	0	320.5
*This particular shearing stiffness was taken to be 90 MPa, as a safe value other than its mean value reported in the molecular simulation study, for the reasons explained in subsection 3.2.												

and the DIM in the direct mode of two-component homogenization takes the following form of mathematical representation

$$\mathcal{C}^{il}=\mathcal{C}^{ref}\left[\mathcal{I}+\left(\left[\eta_{am}\left(\mathcal{S}^{\infty}+\left(\mathcal{C}^{am}-\mathcal{C}^{ref}\right)^{-1}\mathcal{C}^{ref}\right)^{-1}+\eta_{ip}\left(\mathcal{S}^{\infty}+\left(\mathcal{C}^{ip}-\mathcal{C}^{ref}\right)^{-1}\mathcal{C}^{ref}\right)^{-1}\right]^{-1}-\mathcal{S}^{\infty}\right)^{-1}\right] \quad (9)$$

Therefore, once $\mathcal{C}^{ip}$, $\mathcal{C}^{am}$ and their volume fractions are known, the ECIM and the DIM directly return the solution, namely $\mathcal{C}^{il}$, in a single step without requiring any specific numerical technique. Finally, it should be underlined that the interphase stiffness components shown in boldface in Table 1 indicate that $\mathcal{C}^{ip}$ is not positive definite. This finding has been discussed in depth in the following subsections.

3.1. A probe into the shearing components of $\mathcal{C}^{il}$

Due to their critical role in the dissociation analysis, shearing stiffnesses in $\mathcal{C}^{il}$ are examined more closely. The most controversial elements of $\mathcal{C}^{il}$ are C_{44}^{il}, with an uncertainty of $\pm 100\,\text{MPa}$, and C_{55}^{il}, with an uncertainty of $\pm 60\,\text{MPa}$. According to the sensitivity analyses carried out, the following observations were made:

- Variation of C_{44}^{il} within its uncertainty interval brings about the variation of C_{44}^{ip}, C_{46}^{ip} and C_{66}^{ip}, while the other components of $\mathcal{C}^{ip}$ are robust to this variation.
- All components of $\mathcal{C}^{il}$, except for C_{44}^{il}, were allowed to vary within their interval of uncertainty and were observed to affect the value of C_{44}^{ip} only in the tenth decimal place. Similarly, holding C_{55}^{il} fixed and varying the other components of $\mathcal{C}^{il}$ within their uncertainty intervals was observed to affect the value of C_{55}^{ip} only in the sixth decimal place. It can therefore be concluded

that $C_{44}^{\mathrm{ip}}/C_{55}^{\mathrm{ip}}$ is only affected by the uncertainty in the corresponding $C_{44}^{\mathrm{il}}/C_{55}^{\mathrm{il}}$ and is very robust to the uncertainty of the other components of $\mathcal{C}^{\mathrm{il}}$.

- Variation of C_{66}^{il} only varies C_{66}^{ip}, with the other components of $\mathcal{C}^{\mathrm{ip}}$ remaining robust to the fluctuations in C_{66}^{il}.

Accordingly, the diagrams of C_{44}^{ip}, C_{46}^{ip} and C_{66}^{ip} vs. the uncertainty interval of C_{44}^{il} at several temperatures are plotted in Fig. 2, Fig. 3 and Fig. 4, respectively. As is qualitatively evident from the diagrams and as demarcated by vertical dashed lines, there are intervals of C_{44}^{il} for which the dependent variables become unbounded, which is unacceptable. Therefore, these intervals must be excluded from $-100\,\mathrm{MPa} \le C_{44}^{\mathrm{il}} \le 100\,\mathrm{MPa}$. Specifically, Fig. 2, Fig. 3 and Fig. 4 suggest that the imprecise intervals $(2.2,4)$, $(2.5,4)$ and $(-15.5,16)$ must be excluded from the initial interval of C_{44}^{il}. Therefore, the rough interval $-15.5\,\mathrm{MPa} \le C_{44}^{\mathrm{il}} \le 16\,\mathrm{MPa}$, within which $\left|C_{66}^{\mathrm{ip}}\right| > 10000\,\mathrm{MPa}$, is excluded from the initial uncertainty interval of C_{44}^{il}. On the other hand, within $[-100,-15.5]$, $C_{66}^{\mathrm{ip}} > 4000\,\mathrm{MPa}$ which might be considered incomparable with the shearing components of C^{il}. Additionally, it looks rather unusual to assume that the admissible interval of C_{44}^{il} consists of two separate intervals, i.e. $C_{44}^{\mathrm{il}} \in [-100,-15.5] \cup [16,100]$. Therefore, if one sets the criterion for the admissibility of C_{44}^{il} to $\left|C_{66}^{\mathrm{ip}}\right| < 4000\,\mathrm{MPa}$, then the allowable interval of C_{44}^{il} shrinks to $26.5\,\mathrm{MPa} \le C_{44}^{\mathrm{il}} \le 100\,\mathrm{MPa}$ since for $16\,\mathrm{MPa} < C_{44}^{\mathrm{il}} < 26.5\,\mathrm{MPa}$, C_{66}^{ip} takes values less than -4000 MPa.

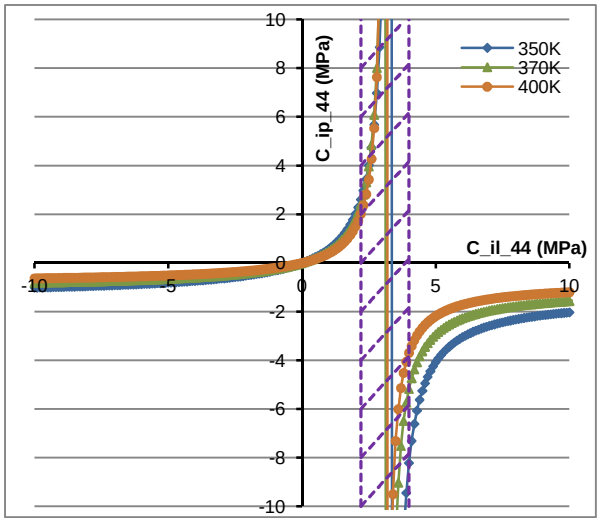

Fig. 2 (color figure) Diagrams of C_{44}^{ip} vs. C_{44}^{il}. Within the approximate interval $(2.2,4)$ delineated by dashed lines, C_{44}^{ip} takes incomparably large value.

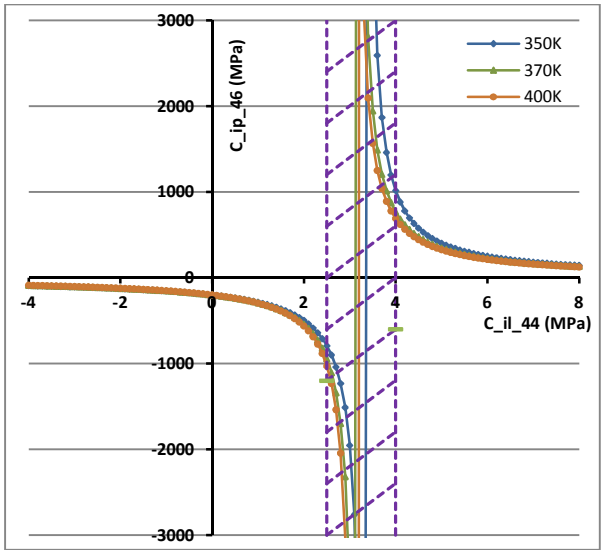

Fig. 3 (color figure) Diagrams of C_{46}^{ip} vs. C_{44}^{il}. Within the approximate interval $(2.5,4)$ delineated by dashed lines, C_{46}^{ip} takes incomparably large value.

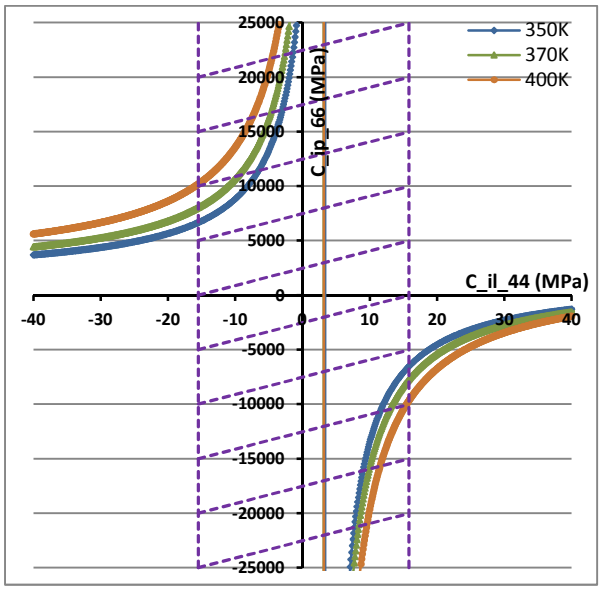

Fig. 4 (color figure) Diagrams of C_{66}^{ip} vs. C_{44}^{il}. Within the approximate interval $(-15.5,16)$ delineated by dashed lines, C_{66}^{ip} takes incomparably large value.

The shearing stiffness C_{55}^{ip} as a function of C_{55}^{il} behaves similar to C_{44}^{ip} as a function of C_{44}^{il}. In other words, for all temperatures within the considered range, C_{55}^{ip} shows a weak dependence on the uncertainty of C_{55}^{il} but is not as robust as it is to the uncertainties of the other components of $\mathscr{C}^{\mathrm{il}}$. The common feature between C_{44}^{ip} and C_{55}^{ip} is that within the temperature range of interest, they robustly take negative values close to zero and exhibit an almost plateau dependence on C_{44}^{il} and C_{55}^{il},

respectively. As demonstrated in Appendix B, this property is insensitive to both the uncertainties of the adopted amorphous elastic parameters and the uncertainties of $\mathcal{C}^{\mathrm{il}}$.

3.2. Deviation of the interphase stiffness from positive definiteness

Positive definiteness of the stiffness tensor for stable materials found in nature is demonstrated based on the first law of thermodynamics and the positivity of the elastic strain energy. If the stiffness tensor is represented in 6×6 matrix form, positive definiteness requires positivity of the diagonal elements. Here, this requirement is violated at least for $\mathcal{C}^{\mathrm{ip}}$ since C_{44}^{ip} and C_{55}^{ip}, although too close to zero, robustly take negative values at least in the temperature range of 350-400 K. It is worth noting that unlike either the crystalline or amorphous phases, the interphase and interlamellar domains are not necessarily thermodynamically stable phases that can ever exist in the absence of the stabilizing influence of the adjoining crystalline lamellae. Thus there is no compelling reason to require their mechanical stability in isolation either. Here, in our example, the negative shear stiffnesses are only observed in the transversal plane of the interphase layer, whose thickness is ~ 1 nm and plays the role of the transition region between the crystallites and the amorphous phase. Moreover, negativity of the shear modulus has been observed earlier for nanoscale domains within an amorphous matrix [33]. Other examples of the studies available in the open literature on the heterogeneous materials containing at least one component with non-positive definite stiffness include [34-38].

It is worth noting that although C_{44}^{ip} and C_{55}^{ip} are negative, they are very close to zero in magnitude, compared to the other stiffnesses. The closeness to zero is such that they can be taken independent of both temperature or the corresponding component in $\mathcal{C}^{\mathrm{il}}$. But the situation for C_{66}^{ip} is totally different (see Fig. 4); since within the interval of $26.5\,\mathrm{MPa}<C_{44}^{\mathrm{il}}<73\,\mathrm{MPa}$, C_{66}^{ip} takes incomparably negative values that are at least three orders of magnitude larger than C_{44}^{ip} or C_{55}^{ip} without displaying any asymptotic behavior. It is reminded that negativity of the shear stiffnesses imply that upon imposition of positive corresponding shear strains, negative stresses will be produced. Then, one may reason that the negligible negativity of C_{44}^{ip} or C_{55}^{ip} produces negligible negative shear stresses, which may be tolerated by the surrounding media. However, the negativity of C_{66}^{ip} is comparatively so large that, even with relatively small positive shear strains, it produces such large negative shear stresses that are not deemed to be balanced by the surrounding media. Additionally, when C_{44}^{il} approaches the right extreme of its allowable interval, the plateau-like behavior of C_{66}^{ip} is observed, supporting the speculation that, contrary to C_{44}^{ip} and C_{55}^{ip}, negative values are not allowed for C_{66}^{ip}; this suggests that the allowable interval for C_{44}^{il} should shrink to $(73,100]$. It might also be argued that since C_{44}^{ip} and C_{55}^{ip} are shearing resistances in the planes normal to the interface but C_{66}^{ip} is the shearing resistance in the plane parallel to the interface, the dissimilarity between their behaviors could be expected.

The sensitivity analysis of C_{66}^{ip} has revealed that this shearing stiffness is robust to the uncertainties of all components of $\mathcal{C}^{\mathrm{il}}$ except for the uncertainties of C_{44}^{il} and C_{66}^{il}. Accordingly, the diagrams of Fig. 5 are plotted as follows: at different temperatures and across the interval of $40\,\mathrm{MPa}<C_{44}^{\mathrm{il}}<100\,\mathrm{MPa}$, C_{66}^{il} is varied within its uncertainty interval to find the minimum values of C_{66}^{ip} at each temperature. Based on the reasoning made in the preceding paragraph vis-à-vis the inadmissibility of negative values

for C_{66}^{ip}, the admissible interval of C_{44}^{il} will be further reduced to $C_{44}^{\mathrm{il}} > 82\,\mathrm{MPa}$. This is the reason why in Table 1 the value of 90 MPa is assigned to C_{44}^{il} instead of its mean value calculated from MC molecular simulations. Consequently, for the rest of the calculations, the mean value and the uncertainty interval of C_{44}^{il} are taken to be 90 MPa and (82,100) MPa, respectively. It is worth noting that the dissociation analysis has the unintended but useful by-product of confining the most uncertain component of $\mathcal{C}^{\mathrm{il}}$.

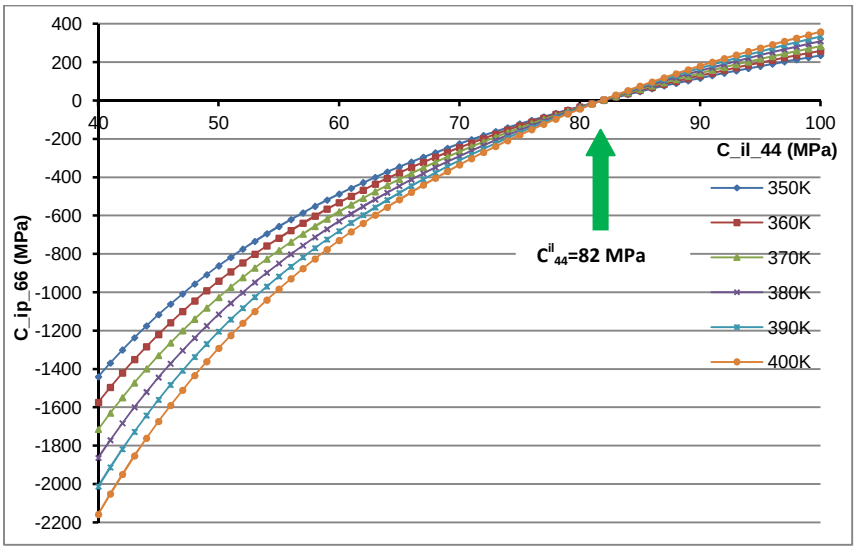

Fig. 5 Diagrams of the minimum values of C_{66}^{ip} vs. C_{44}^{il} at different temperatures. The arrow indicates the threshold value $C_{44}^{\mathrm{il}} = 82\,\mathrm{MPa}$ above which $C_{66}^{\mathrm{ip}} > 0$.

3.3. Verification of our results

Crist et. al [21] reported their measurements for different samples of PE, linear HPB, 3S HPB and 4S HPB spanning a crystallinity range of $0.35 < \xi < 0.68$, which they were able to describe with a linear fit on a semilogarithmic scale with the correlation coefficient of 0.974. Assuming essentially only a two-component model comprising crystalline and noncrystalline (which they call amorphous) phases, they argue that in semi-crystalline PE, the average Young's modulus of the noncrystalline phase is nearly constant (~ 300 MPa) for $\xi > 0.7$, but drops appreciably as crystallinity is lowered below 70%. Therein, they proposed the following double-argument dependence for the average Young's modulus of the noncrystalline phase at room temperature

$$\bar{E}_{\mathrm{am}}(\xi) = \begin{cases} 2\exp(7.158\xi) & \xi \le 0.7 \\ 300 & \xi \ge 0.7 \end{cases} \mathrm{MPa} \qquad (10)$$

Given that Crist and co-workers did not consider the presence of a third component, i.e. the transitional interphase separating crystallites and the central amorphous phase, it is reasonable to equate $\bar{E}_{\mathrm{am}}$ in their two-component model with $\bar{E}_{\mathrm{il}}$. Indeed, $\bar{E}_{\mathrm{il}}$ is calculable form $\mathcal{C}^{\mathrm{il}}$ which is, according to Eq.(1), a function of the properties and volume fractions of its constituents. Therefore, mathematically speaking

$$\bar{E}_{\mathrm{il}} = \psi\left(\eta_{\mathrm{ip}}, \mathcal{C}^{\mathrm{ip}}, \mathcal{C}^{\mathrm{am}}\right) \qquad (11)$$

which is in agreement with the suggestion made by Crist et. al. [21] since η_{ip}, which denotes the interphase volume fraction within the interlamellar domain, is in its turn a function of crystallinity. In other words, for an interlamellar region of arbitrary thickness one can write

$$\eta_{ip} = \frac{2V_{ip}}{2V_{ip}+V_{am}} \simeq \frac{2t_{ip}}{2t_{ip}+t_{am}} \tag{12}$$

where t_{ip}/V_{ip} denotes the thickness/total volume of each interphase layer in a layered, "sandwich" model of the interlamellar domain. There is evidence that the interphase thickness is invariant with crystallinity, whereas the amorphous thickness varies to accommodate changes in interlamellar separation [39]. Consequently t_{am} or equally η_{ip} is a function of crystallinity:

$$\eta_{ip} = h(\xi) \tag{13}$$

For the hypothetical state of no crystallinity, PE is composed of pure amorphous phase and there is no interphase which means:

$$\text{as} \qquad \xi \to 0 \qquad \begin{cases} \eta_{ip} \to 0 \;\; \Rightarrow \;\; \eta_{am} = 1-\eta_{ip} \to 1 \\ \bar{E}_{PE} = \bar{E}_{il} = E_{am} \end{cases} \tag{14}$$

where at room temperature E_{am} takes values between 2-11.4 MPa, as elaborated in subsection 2.1. On the other hand, at high crystallinities, the amorphous phase disappears and the interlamellar domain will be dominated by the interphase layers, meaning that

$$\text{as} \qquad \xi \to 1 \qquad \begin{cases} \eta_{ip} \to 1 \;\; \Rightarrow \;\; \eta_{am} = 1-\eta_{ip} \to 0 \\ \bar{E}_{il} = \bar{E}_{ip} \end{cases} \tag{15}$$

In summary, by increasing the crystallinity from zero, the interphase layers start to appear and the amorphous phase shrinks, implying that η_{ip} is a positive and monotonically increasing function of crystallinity up to some critical crystallinity, ξ_{cr}. Since η_{ip} cannot exceed unity in the interval of $0<\xi<1$ and eventually it has to go to unity as $\xi \to 1$, the most likely dependence form of η_{ip}, which is in accord with the observation by Crist et. al. [21], is that:

η_{ip} increases monotonically from zero at the hypothetical $\xi = 0$ to reach a maximum at the critical $0<\xi_{cr} \sim 0.7<1$ and then plateaus quickly but smoothly such that $\eta_{ip}(\xi > \xi_{cr}) \simeq \eta_{ip}(\xi_{cr})$.

Consequently and in light of Eq.(11), the average Young's modulus of the interlamellar domain, $\bar{E}_{il}$, becomes a function of crystallinity similar to that suggested by Crist et. al. [21], while the constitutive properties of the constituents, namely $\mathcal{C}^{ip}$ and $\mathcal{C}^{am}$, remain essentially independent of crystallinity. In other words, using a two-phase sandwich model to represent the interlamellar region in which the constitutive properties of the phases are independent of crystallinity, the form of dependence in Eq.(10) proposed by Crist et. al. [21] can be justified.

Finally, to use the empirical Eq.(10) for verification purposes, one can reason that according to Eq.(15), at high crystallinity $\overline{E}_{\text{il}} \simeq \overline{E}_{\text{ip}}$, therefore the average Young's modulus of the interphase layer at room temperature must be comparable to that of the interlamellar domain at high crystallinity, which is offered by the empirical relation (10). Following the idea presented by Counts et al. [40], Hill's estimate [41] is utilized to find an estimate for $\overline{E}_{\text{ip}}$ from $\mathcal{C}^{\text{ip}}$. In the work of Counts et al. [40] the problem of estimating the overall shear and Young's moduli of a polycrystalline BCC Mg-Li, which takes non-positive definite stiffnesses for some compositions of Mg-Li, is treated similarly. In fact, their FEM and self-consistent results for the average elastic moduli, when extrapolated to unstable regions, agree very well with the Hill's estimate for any composition. Therefore, in order to estimate the interphase average bulk and shear moduli using Hill's method, the bulk and shear moduli of the Voigt and Reuss approaches, calculable from $\left\langle \mathcal{C}^{\text{ip}} \right\rangle$ and $\left\langle \mathcal{C}^{\text{ip}^{-1}} \right\rangle^{-1}$ where $\langle\ \rangle$ indicates the orientational (volume) averaging, are required. Thus, Hill's estimates of the interphase bulk and shear moduli are obtained as follows:

$$\begin{aligned} \overline{\kappa}_{\text{ip-Hill}} &= \frac{1}{2}\left(\overline{\kappa}_{\text{ip-V}} + \overline{\kappa}_{\text{ip-R}}\right) \\ \overline{G}_{\text{ip-Hill}} &= \frac{1}{2}\left(\overline{G}_{\text{ip-V}} + \overline{G}_{\text{ip-R}}\right) \end{aligned} \tag{16}$$

from which the average Young's modulus of the interphase reads

$$\overline{E}_{\text{ip-Hill}} = \frac{9\,\overline{\kappa}_{\text{ip-Hill}}\,\overline{G}_{\text{ip-Hill}}}{3\,\overline{\kappa}_{\text{ip-Hill}} + \overline{G}_{\text{ip-Hill}}} \tag{17}$$

In the temperature range studied here, the closest to the room temperature is 350 K at which $\overline{E}_{\text{ip-Hill}}$ is calculated to be 347 MPa, which compares well to the plateau value of 300 MPa proposed by Crist et. al. [21] noting that the Young's modulus of amorphous polymers increases with temperature if the polymer is in the rubbery state. Furthermore, Ding et al. [42] conducted a molecular simulation study on the Young's modulus change in a semi-crystalline polymer and observed that the Young's modulus of the interlamellar region increases with temperature in the rubbery state. It is therefore expected that the analogue of the empirical relation (10) at higher temperatures gives higher $\overline{E}_{\text{il}}$ for the same crystallinity. As a result, $\overline{E}_{\text{ip}}$ at 350 K ought to be greater than 300 MPa. Additionally, keeping in mind that the components of $\mathcal{C}^{\text{ip}}$ have uncertainty intervals inherited from the uncertainties of $\mathcal{C}^{\text{il}}$ components, the calculated $\overline{E}_{\text{ip-Hill}}$ will definitely have its own uncertainty interval. By means of a simple Monte Carlo analysis sampling 10^9 times the uncertainty space of $\mathcal{C}^{\text{il}}$ and then calculating new $\mathcal{C}^{\text{ip}}$s and new $\overline{E}_{\text{ip-Hill}}$s at 350 K, the following uncertainty interval for $\overline{E}_{\text{ip-Hill}}$ is obtained:

$$207\,\text{MPa} < \overline{E}_{\text{ip-Hill}}\Big|_{350\,\text{K}} < 465\,\text{MPa} \tag{18}$$

This result is in accord with our expectation that the values higher than 300 MPa fall within the uncertainty interval of $\overline{E}_{\text{ip-Hill}}$. It is reiterated that for calculating the mean value of $\overline{E}_{\text{ip-Hill}}$ and its uncertainty interval, it was assumed that $82\,\text{MPa} < C_{44}^{\text{il}} \le 100\,\text{MPa}$ with a means value of $C_{44}^{\text{il}} = 90\,\text{MPa}$.

4. Summary and Conclusion

In this study, a methodology is presented for the mechanical characterization of the interphase layer in semi-crystalline PE, which is based on applying micromechanical homogenization techniques to the data from the Monte Carlo molecular simulations of the noncrystalline domain in PE. To this end, two micromechanical homogenization approaches of DIM and ECIM were reversely applied to the molecular simulation results of the interlamellar region across the temperature range of 350K-400K. The outputs of both approaches are identical despite their nonidentical contexts; confirming the outputs of the implemented dissociation methodology.

As a requirement for implementing the dissociation analysis, the stiffness tensor of the amorphous phase has been estimated by relying on the findings of several independent experimental studies. The dissociation analysis revealed that the interphase shearing stiffnesses in planes normal to the interface, i.e. C_{44}^{ip} and C_{55}^{ip}, robustly take small but negative values, leading to the non-positive definiteness of the interphase stiffness tensor, at least, for the temperature range of interest. We believe that this non-positive definiteness is a valid outcome whose origin lies in the fact that the interphase is a transitional domain whose existence is always accompanied by neighboring crystalline and amorphous phases that mechanically stabilize the interphase. Contrary to the two other shearing stiffnesses, C_{66}^{ip} shows a different behavior, due possibly to its resistance in the plane parallel to the interface. After running a specific sensitivity analysis (given in Appendix B), we could ascertain the insensitivity of the non-positive definiteness of $\mathcal{C}^{\mathrm{ip}}$ from the uncertainties of the adopted amorphous elastic constants, for the temperature range of 350 K-400 K.

The dissociation analysis has had the favorable advantage of constraining the most uncertain component of the initial interlamellar stiffness, C_{44}^{il}. As another finding, it has been found that for dissociation purposes the DIM works perfectly without posing any numerical problems while the ECIM is either prone to numerical divergence problems if the recursive method is used or demands time-consuming optimization algorithms. In the homogenization mode, however, both approaches are equally fast and devoid of any numerical problems.

Finally, using the proposed two-component sandwich model a plausible explanation has been suggested for an empirical relation that describes the interlamellar average Young's modulus as a function of crystallinity. In the explanation provided, the constitutive properties of the composing phases are invariant with crystallinity while only the volume fractions vary with crystallinity. On the other hand, since at high crystallinities the interlamellar region is dominated by the interphase layer, the average Young's modulus of the interphase should be comparable to that of the interlamellar domain at high crystallinities. Without taking the impact of uncertainties into account, Hill's estimate of the interphase average Young's modulus at 350 K is 347 MPa. This mean value compares well with the empirical value of 300 MPa in addition to being consistent with the established fact that the elastic modulus of a rubbery amorphous polymer increases with temperature. This good agreement endorses the tailored methodology and the dissociation results.

Acknowledgment

A. Gh. thanks the Cultural Department of the French Embassy in Tehran and the French Government for financial support provided within the "Bourse de Cotutelle" program.

Appendix A

The extended version of the composite inclusion model (ECIM)

The original version of the composite inclusion model (CIM) was an effort to attain a more realistic estimation of the effective stiffness of a two-layer composite inclusion than those suggested by Voigt and Reuss models [31,32]. In light of the notion presented therein, this approach is extended to calculate the effective stiffness/compliance of a three-layer composite inclusion.

The schematic of a three-layer composite inclusion is depicted in Fig. B.1. From the average theorems, the average stress and strain of this composite inclusion, $\overline{\boldsymbol{\sigma}}^{\mathrm{I}}$ and $\overline{\boldsymbol{\varepsilon}}^{\mathrm{I}}$, are expressed as

$$\overline{\boldsymbol{\sigma}}^{\mathrm{I}} = \eta_1 \overline{\boldsymbol{\sigma}}^{1} + \eta_2 \overline{\boldsymbol{\sigma}}^{2} + \eta_3 \overline{\boldsymbol{\sigma}}^{3} \tag{A.1}$$

$$\overline{\boldsymbol{\varepsilon}}^{\mathrm{I}} = \eta_1 \overline{\boldsymbol{\varepsilon}}^{1} + \eta_2 \overline{\boldsymbol{\varepsilon}}^{2} + \eta_3 \overline{\boldsymbol{\varepsilon}}^{3} \tag{A.2}$$

where η_{i}, $\overline{\boldsymbol{\sigma}}^{\mathrm{i}}$ and $\overline{\boldsymbol{\varepsilon}}^{\mathrm{i}}$ stand respectively for the volume fraction, average stress and average strain of the *i*th layer/phase, with $\mathrm{i}=1,2,3$. Let us assume that the governing linear elastic constitutive law for each phase follows as

$$\overline{\boldsymbol{\varepsilon}}^{\mathrm{i}} = \mathcal{S}^{\mathrm{i}} \overline{\boldsymbol{\sigma}}^{\mathrm{i}} \qquad \text{or} \qquad \overline{\boldsymbol{\sigma}}^{\mathrm{i}} = \mathcal{C}^{\mathrm{i}} \overline{\boldsymbol{\varepsilon}}^{\mathrm{i}} \qquad \text{with} \quad \mathcal{S}^{\mathrm{i}} = \left(\mathcal{C}^{\mathrm{i}}\right)^{-1} \tag{A.3}$$

where $\mathcal{S}^{\mathrm{i}}$ and $\mathcal{C}^{\mathrm{i}}$ are, respectively, the compliance and stiffness of the *i*th phase. If the effective compliance and stiffness of the three-layer inclusion are defined as coefficients correlating $\overline{\boldsymbol{\sigma}}^{\mathrm{I}}$ and $\overline{\boldsymbol{\varepsilon}}^{\mathrm{I}}$ as follows:

$$\overline{\boldsymbol{\varepsilon}}^{\mathrm{I}} = \mathcal{S}^{\mathrm{I}} \overline{\boldsymbol{\sigma}}^{\mathrm{I}} \qquad \text{or} \qquad \overline{\boldsymbol{\sigma}}^{\mathrm{I}} = \mathcal{C}^{\mathrm{I}} \overline{\boldsymbol{\varepsilon}}^{\mathrm{I}} \qquad \text{with} \quad \mathcal{S}^{\mathrm{I}} = \left(\mathcal{C}^{\mathrm{I}}\right)^{-1}, \tag{A.4}$$

then substitution of (A.3) and (A.4) into (A.1) and (A.2) yields

$$\mathcal{C}^{\mathrm{I}} = \eta_1 \mathcal{C}^{1} \mathcal{Q}^{1} + \eta_2 \mathcal{C}^{2} \mathcal{Q}^{2} + \eta_3 \mathcal{C}^{3} \mathcal{Q}^{3} \tag{A.5}$$

$$\mathcal{S}^{\mathrm{I}} = \eta_1 \mathcal{S}^{1} \mathcal{R}^{1} + \eta_2 \mathcal{S}^{2} \mathcal{R}^{2} + \eta_3 \mathcal{S}^{3} \mathcal{R}^{3}, \tag{A.6}$$

where the weight functions $\mathcal{Q}^{\mathrm{i}}$ and $\mathcal{R}^{\mathrm{i}}$, called strain and stress concentrations, respectively, are defined as

$$\overline{\boldsymbol{\varepsilon}}^{\mathrm{i}} = \mathcal{Q}^{\mathrm{i}} \overline{\boldsymbol{\varepsilon}}^{\mathrm{I}} \tag{A.7}$$

$$\overline{\boldsymbol{\sigma}}^{\mathrm{i}} = \mathcal{R}^{\mathrm{i}} \overline{\boldsymbol{\sigma}}^{\mathrm{I}} \tag{A.8}$$

Therefore, once the stress or strain concentrations are determined, the effective stiffness/compliance of the composite inclusion is calculable. An important auxiliary assumption of CIM that is not explicitly stated in [31,32] but is invoked implicitly is that the stress and strain in each phase are assumed to be uniform. This assumption, in conjunction with the enforcement of the equilibrium conditions at the two interfaces, gives rise to

$$\overline{\boldsymbol{\sigma}}_{\beta}^{1} = \overline{\boldsymbol{\sigma}}_{\beta}^{2} = \overline{\boldsymbol{\sigma}}_{\beta}^{3} = \overline{\boldsymbol{\sigma}}_{\beta}^{\mathrm{I}} \tag{A.9}$$

where $\beta = 3,4,5$. In Eq. (A.9) the Voigt contracted notation is used in addition to the assumption that, in conformity with the convention adopted in [20,31,32], the interfaces are parallel to the 12-plane, consequently the 3-axis is normal to the interfaces (see Fig. B.1). By substitution of (A.9) into (A.8) there obtains

$$\overline{\boldsymbol{\sigma}}_{\beta}^{\mathrm{i}} = \mathscr{R}_{\beta \mathrm{j}}^{\mathrm{i}} \overline{\boldsymbol{\sigma}}_{\mathrm{j}}^{\mathrm{I}} = \overline{\boldsymbol{\sigma}}_{\beta}^{\mathrm{I}} \qquad \rightarrow \qquad \mathscr{R}_{\beta \mathrm{j}}^{\mathrm{i}} = \boldsymbol{\delta}_{\beta \mathrm{j}} \tag{A.10}$$

where $\boldsymbol{\delta}$ denotes the extended Kronecker delta. Compatibility conditions at the interfaces, along with the assumption of uniformity of strains in each phase, require that if $\alpha = 1,2,6$ then

$$\overline{\boldsymbol{\varepsilon}}_{\alpha}^{1} = \overline{\boldsymbol{\varepsilon}}_{\alpha}^{2} = \overline{\boldsymbol{\varepsilon}}_{\alpha}^{3} = \overline{\boldsymbol{\varepsilon}}_{\alpha}^{\mathrm{I}} \tag{A.11}$$

or equally

$$\mathscr{S}_{\alpha \mathrm{j}}^{1} \overline{\boldsymbol{\sigma}}_{\mathrm{j}}^{1} = \mathscr{S}_{\alpha \mathrm{j}}^{2} \overline{\boldsymbol{\sigma}}_{\mathrm{j}}^{2} = \mathscr{S}_{\alpha \mathrm{j}}^{3} \overline{\boldsymbol{\sigma}}_{\mathrm{j}}^{3} \tag{A.12}$$

where in combination with (A.1) results in

$$\begin{aligned} &\mathscr{S}_{\alpha \mathrm{j}}^{1} \overline{\boldsymbol{\sigma}}_{\mathrm{j}}^{1} = \frac{1}{\eta_2} \mathscr{S}_{\alpha \mathrm{j}}^{2} \left(\overline{\boldsymbol{\sigma}}_{\mathrm{j}}^{\mathrm{I}} - \eta_1 \overline{\boldsymbol{\sigma}}_{\mathrm{j}}^{1} - \eta_3 \overline{\boldsymbol{\sigma}}_{\mathrm{j}}^{3} \right) \\ &\eta_2 \mathscr{S}_{\alpha \mathrm{j}}^{1} \overline{\boldsymbol{\sigma}}_{\mathrm{j}}^{1} + \eta_1 \mathscr{S}_{\alpha \mathrm{j}}^{2} \overline{\boldsymbol{\sigma}}_{\mathrm{j}}^{1} + \eta_3 \mathscr{S}_{\alpha \mathrm{j}}^{2} \overline{\boldsymbol{\sigma}}_{\mathrm{j}}^{3} = \mathscr{S}_{\alpha \mathrm{j}}^{2} \overline{\boldsymbol{\sigma}}_{\mathrm{j}}^{\mathrm{I}} \end{aligned} \tag{A.13}$$

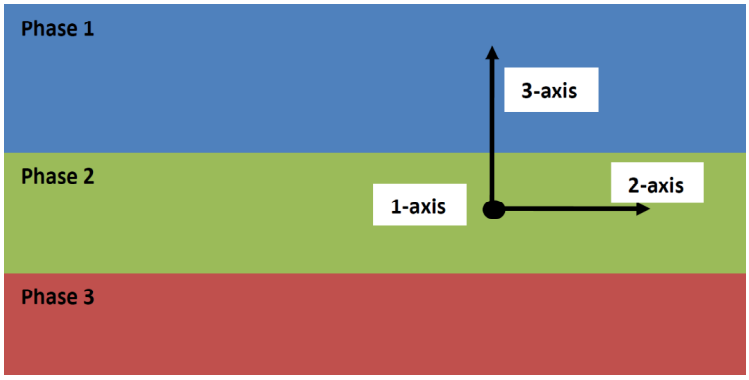

Fig. B.1 (color figure) Schematic of a three-layer composite inclusion along with the relative orientation of the selected reference frame

Further decomposition of (A.13) gives

$$\begin{aligned} &\eta_2 \left(\mathscr{S}_{\alpha\alpha'}^{1} \overline{\boldsymbol{\sigma}}_{\alpha'}^{1} + \mathscr{S}_{\alpha\beta'}^{1} \overline{\boldsymbol{\sigma}}_{\beta'}^{1} \right) + \eta_1 \left(\mathscr{S}_{\alpha\alpha'}^{2} \overline{\boldsymbol{\sigma}}_{\alpha'}^{1} + \mathscr{S}_{\alpha\beta'}^{2} \overline{\boldsymbol{\sigma}}_{\beta'}^{1} \right) + \eta_3 \left(\mathscr{S}_{\alpha\alpha'}^{2} \overline{\boldsymbol{\sigma}}_{\alpha'}^{3} + \mathscr{S}_{\alpha\beta'}^{2} \overline{\boldsymbol{\sigma}}_{\beta'}^{3} \right) = \mathscr{S}_{\alpha \mathrm{j}}^{2} \overline{\boldsymbol{\sigma}}_{\mathrm{j}}^{\mathrm{I}} \\ &\left(\eta_2 \mathscr{S}_{\alpha\alpha'}^{1} + \eta_1 \mathscr{S}_{\alpha\alpha'}^{2} \right) \overline{\boldsymbol{\sigma}}_{\alpha'}^{1} + \left(\eta_2 \mathscr{S}_{\alpha\beta'}^{1} + \eta_1 \mathscr{S}_{\alpha\beta'}^{2} \right) \overline{\boldsymbol{\sigma}}_{\beta'}^{1} + \eta_3 \mathscr{S}_{\alpha\alpha'}^{2} \overline{\boldsymbol{\sigma}}_{\alpha'}^{3} + \eta_3 \mathscr{S}_{\alpha\beta'}^{2} \overline{\boldsymbol{\sigma}}_{\beta'}^{3} = \mathscr{S}_{\alpha \mathrm{j}}^{2} \overline{\boldsymbol{\sigma}}_{\mathrm{j}}^{\mathrm{I}} \end{aligned} \tag{A.14}$$

where $\alpha' = 1,2,6$ and $\beta' = 3,4,5$. To eliminate $\boldsymbol{\sigma}_{\alpha'}^{3}$ from Eq.(A.14), Eqs.(A.2) and (A.3) are exploited to obtain

$$\begin{aligned} &\mathscr{S}_{\alpha\alpha'}^{1} \overline{\boldsymbol{\sigma}}_{\alpha'}^{1} + \mathscr{S}_{\alpha\beta'}^{1} \overline{\boldsymbol{\sigma}}_{\beta'}^{1} = \mathscr{S}_{\alpha\alpha'}^{3} \overline{\boldsymbol{\sigma}}_{\alpha'}^{3} + \mathscr{S}_{\alpha\beta'}^{3} \overline{\boldsymbol{\sigma}}_{\beta'}^{3} \\ &\overline{\boldsymbol{\sigma}}_{\alpha'}^{3} = \left(\mathscr{S}_{\alpha\alpha'}^{3} \right)^{-1} \left(\mathscr{S}_{\alpha\alpha'}^{1} \overline{\boldsymbol{\sigma}}_{\alpha'}^{1} + \left(\mathscr{S}_{\alpha\beta'}^{1} - \mathscr{S}_{\alpha\beta'}^{3} \right) \overline{\boldsymbol{\sigma}}_{\beta'}^{1} \right) \end{aligned} \tag{A.15}$$

Simultaneous use of Eqs.(A.14) and (A.15) yields

$$\begin{aligned}
&\left(\eta_2\mathcal{S}^1_{\alpha\alpha'}+\eta_1\mathcal{S}^2_{\alpha\alpha'}\right)\bar{\boldsymbol{\sigma}}^1_{\alpha'}+\left(\eta_2\mathcal{S}^1_{\alpha\beta'}+\eta_1\mathcal{S}^2_{\alpha\beta'}+\eta_3\mathcal{S}^2_{\alpha\beta'}\right)\bar{\boldsymbol{\sigma}}^1_{\beta'}+\\
&\eta_3\mathcal{S}^2_{\alpha\alpha'}\left(\mathcal{S}^3_{\alpha\alpha'}\right)^{-1}\mathcal{S}^1_{\alpha\alpha'}\bar{\boldsymbol{\sigma}}^1_{\alpha'}+\eta_3\mathcal{S}^2_{\alpha\alpha'}\left(\mathcal{S}^3_{\alpha\alpha'}\right)^{-1}\left(\mathcal{S}^1_{\alpha\beta'}-\mathcal{S}^3_{\alpha\beta'}\right)\bar{\boldsymbol{\sigma}}^1_{\beta'}=\\
&\left(\eta_2\mathcal{S}^1_{\alpha\alpha'}+\eta_1\mathcal{S}^2_{\alpha\alpha'}+\eta_3\mathcal{S}^2_{\alpha\alpha'}\left(\mathcal{S}^3_{\alpha\alpha'}\right)^{-1}\mathcal{S}^1_{\alpha\alpha'}\right)\bar{\boldsymbol{\sigma}}^1_{\alpha'}+\left(\eta_2\mathcal{S}^1_{\alpha\beta'}+\eta_1\mathcal{S}^2_{\alpha\beta'}+\eta_3\mathcal{S}^2_{\alpha\beta'}+\eta_3\mathcal{S}^2_{\alpha\alpha'}\left(\mathcal{S}^3_{\alpha\alpha'}\right)^{-1}\left(\mathcal{S}^1_{\alpha\beta'}-\mathcal{S}^3_{\alpha\beta'}\right)\right)\bar{\boldsymbol{\sigma}}^1_{\beta'}=\mathcal{S}^2_{\alpha\mathrm{j}}\bar{\boldsymbol{\sigma}}^{\mathrm{I}}_{\mathrm{j}}
\end{aligned}\tag{A.16}$$

or equally

$$\begin{aligned}
&\left(\eta_2\mathcal{S}^1_{\alpha\alpha'}+\eta_1\mathcal{S}^2_{\alpha\alpha'}+\eta_3\mathcal{S}^2_{\alpha\alpha'}\left(\mathcal{S}^3_{\alpha\alpha'}\right)^{-1}\mathcal{S}^1_{\alpha\alpha'}\right)\bar{\boldsymbol{\sigma}}^1_{\alpha'}+\left(\eta_2\mathcal{S}^1_{\alpha\beta'}+\eta_1\mathcal{S}^2_{\alpha\beta'}+\eta_3\mathcal{S}^2_{\alpha\beta'}+\eta_3\mathcal{S}^2_{\alpha\alpha'}\left(\mathcal{S}^3_{\alpha\alpha'}\right)^{-1}\left(\mathcal{S}^1_{\alpha\beta'}-\mathcal{S}^3_{\alpha\beta'}\right)\right)\bar{\boldsymbol{\sigma}}^1_{\beta'}=\mathcal{S}^2_{\alpha\mathrm{j}}\bar{\boldsymbol{\sigma}}^{\mathrm{I}}_{\mathrm{j}}\\
&\bar{\boldsymbol{\sigma}}^1_{\alpha'}=\left(\eta_2\mathcal{S}^1_{\alpha\alpha'}+\eta_1\mathcal{S}^2_{\alpha\alpha'}+\eta_3\mathcal{S}^2_{\alpha\alpha'}\left(\mathcal{S}^3_{\alpha\alpha'}\right)^{-1}\mathcal{S}^1_{\alpha\alpha'}\right)^{-1}\left[\mathcal{S}^2_{\alpha\mathrm{j}}-\left(\eta_2\mathcal{S}^1_{\alpha\beta'}+\eta_1\mathcal{S}^2_{\alpha\beta'}+\eta_3\mathcal{S}^2_{\alpha\beta'}+\eta_3\mathcal{S}^2_{\alpha\alpha'}\left(\mathcal{S}^3_{\alpha\alpha'}\right)^{-1}\left(\mathcal{S}^1_{\alpha\beta'}-\mathcal{S}^3_{\alpha\beta'}\right)\right)\boldsymbol{\delta}_{\beta'\mathrm{j}}\right]\bar{\boldsymbol{\sigma}}^{\mathrm{I}}_{\mathrm{j}}
\end{aligned}\tag{A.17}$$

Accordingly,

$$\mathcal{R}^1_{\alpha\mathrm{j}}=\left(\eta_2\mathcal{S}^1_{\alpha\alpha'}+\eta_1\mathcal{S}^2_{\alpha\alpha'}+\eta_3\mathcal{S}^2_{\alpha\alpha'}\left(\mathcal{S}^3_{\alpha\alpha'}\right)^{-1}\mathcal{S}^1_{\alpha\alpha'}\right)^{-1}\left[\mathcal{S}^2_{\alpha\mathrm{j}}-\left(\eta_2\mathcal{S}^1_{\alpha\beta'}+\eta_1\mathcal{S}^2_{\alpha\beta'}+\eta_3\mathcal{S}^2_{\alpha\beta'}+\eta_3\mathcal{S}^2_{\alpha\alpha'}\left(\mathcal{S}^3_{\alpha\alpha'}\right)^{-1}\left(\mathcal{S}^1_{\alpha\beta'}-\mathcal{S}^3_{\alpha\beta'}\right)\right)\boldsymbol{\delta}_{\beta'\mathrm{j}}\right]\tag{A.18}$$

In a similar way, the two other stress concentrations are obtained as follows

$$\mathcal{R}^2_{\alpha\mathrm{j}}=\left(\eta_1\mathcal{S}^2_{\alpha\alpha'}+\eta_2\mathcal{S}^1_{\alpha\alpha'}+\eta_3\mathcal{S}^1_{\alpha\alpha'}\left(\mathcal{S}^3_{\alpha\alpha'}\right)^{-1}\mathcal{S}^2_{\alpha\alpha'}\right)^{-1}\left[\mathcal{S}^1_{\alpha\mathrm{j}}-\left(\eta_1\mathcal{S}^2_{\alpha\beta'}+\eta_2\mathcal{S}^1_{\alpha\beta'}+\eta_3\mathcal{S}^1_{\alpha\beta'}+\eta_3\mathcal{S}^1_{\alpha\alpha'}\left(\mathcal{S}^3_{\alpha\alpha'}\right)^{-1}\left(\mathcal{S}^2_{\alpha\beta'}-\mathcal{S}^3_{\alpha\beta'}\right)\right)\boldsymbol{\delta}_{\beta'\mathrm{j}}\right]\tag{A.19}$$

$$\mathcal{R}^3_{\alpha\mathrm{j}}=\left(\eta_2\mathcal{S}^3_{\alpha\alpha'}+\eta_3\mathcal{S}^2_{\alpha\alpha'}+\eta_1\mathcal{S}^2_{\alpha\alpha'}\left(\mathcal{S}^1_{\alpha\alpha'}\right)^{-1}\mathcal{S}^3_{\alpha\alpha'}\right)^{-1}\left[\mathcal{S}^2_{\alpha\mathrm{j}}-\left(\eta_2\mathcal{S}^3_{\alpha\beta'}+\eta_3\mathcal{S}^2_{\alpha\beta'}+\eta_1\mathcal{S}^2_{\alpha\beta'}+\eta_1\mathcal{S}^2_{\alpha\alpha'}\left(\mathcal{S}^1_{\alpha\alpha'}\right)^{-1}\left(\mathcal{S}^3_{\alpha\beta'}-\mathcal{S}^1_{\alpha\beta'}\right)\right)\boldsymbol{\delta}_{\beta'\mathrm{j}}\right]\tag{A.20}$$

The elements of the six-by-six stress concentrations are now determined and can be substituted in Eq.(A.6) for the calculation of the effective compliance. A similar procedure can be followed for the derivation of the strain concentrations, leading to

$$\mathcal{Q}^{\mathrm{i}}_{\alpha\mathrm{j}}=\boldsymbol{\delta}_{\alpha\mathrm{j}}\tag{A.21}$$

$$\mathcal{Q}^1_{\beta\mathrm{j}}=\left[\eta_1\mathcal{C}^2_{\beta\beta'}+\eta_2\mathcal{C}^1_{\beta\beta'}+\eta_3\mathcal{C}^2_{\beta\beta'}\left(\mathcal{C}^3_{\beta\beta'}\right)^{-1}\mathcal{C}^1_{\beta\beta'}\right]^{-1}\left[\mathcal{C}^2_{\beta\beta'}\boldsymbol{\delta}_{\beta\mathrm{j}}-\left[\eta_2\left(\mathcal{C}^1_{\beta\alpha'}-\mathcal{C}^2_{\beta\alpha'}\right)+\eta_3\mathcal{C}^2_{\beta\beta'}\left(\mathcal{C}^3_{\beta\beta'}\right)^{-1}\left(\mathcal{C}^1_{\beta\alpha'}-\mathcal{C}^3_{\beta\alpha'}\right)\right]\boldsymbol{\delta}_{\alpha\mathrm{j}}\right]\tag{A.22}$$

$$\mathcal{Q}^2_{\beta\mathrm{j}}=\left[\eta_2\mathcal{C}^1_{\beta\beta'}+\eta_1\mathcal{C}^2_{\beta\beta'}+\eta_3\mathcal{C}^1_{\beta\beta'}\left(\mathcal{C}^3_{\beta\beta'}\right)^{-1}\mathcal{C}^2_{\beta\beta'}\right]^{-1}\left[\mathcal{C}^1_{\beta\beta'}\boldsymbol{\delta}_{\beta\mathrm{j}}-\left[\eta_1\left(\mathcal{C}^2_{\beta\alpha'}-\mathcal{C}^1_{\beta\alpha'}\right)+\eta_3\mathcal{C}^1_{\beta\beta'}\left(\mathcal{C}^3_{\beta\beta'}\right)^{-1}\left(\mathcal{C}^2_{\beta\alpha'}-\mathcal{C}^3_{\beta\alpha'}\right)\right]\boldsymbol{\delta}_{\alpha\mathrm{j}}\right]\tag{A.23}$$

$$\mathcal{Q}^3_{\beta\mathrm{j}}=\left[\eta_3\mathcal{C}^2_{\beta\beta'}+\eta_2\mathcal{C}^3_{\beta\beta'}+\eta_1\mathcal{C}^2_{\beta\beta'}\left(\mathcal{C}^1_{\beta\beta'}\right)^{-1}\mathcal{C}^3_{\beta\beta'}\right]^{-1}\left[\mathcal{C}^2_{\beta\beta'}\boldsymbol{\delta}_{\beta\mathrm{j}}-\left[\eta_2\left(\mathcal{C}^3_{\beta\alpha'}-\mathcal{C}^2_{\beta\alpha'}\right)+\eta_1\mathcal{C}^2_{\beta\beta'}\left(\mathcal{C}^1_{\beta\beta'}\right)^{-1}\left(\mathcal{C}^3_{\beta\alpha'}-\mathcal{C}^1_{\beta\alpha'}\right)\right]\boldsymbol{\delta}_{\alpha\mathrm{j}}\right]\tag{A.24}$$

It is worth mentioning that the Gueguen et al. [16] have also tried to derive similar relationships for the stress and strain concentrations but made errors, ending up with erroneous relationships.

In our example of the interlamellar region, the properties of phase 1 and phase 3 are identical as they represent the side interphase layers. Therefore, Eq.(A.6) is rewritten as follows:

$$\left(\mathcal{C}^{\mathrm{I}}\right)^{-1}=\mathcal{S}^{\mathrm{I}}=2\eta_1\left(\mathcal{C}^1\right)^{-1}\mathcal{R}^1+\eta_2\left(\mathcal{C}^2\right)^{-1}\mathcal{R}^2\tag{A.25}$$

In the above equation, the unknown is $\mathcal{C}^1 = \mathcal{C}^{\text{ip}}$. On the other hand, $\mathcal{R}^1$ and $\mathcal{R}^2$ are non-linear tensorial functions of $\mathcal{C}^1$, $\mathcal{C}^2 = \mathcal{C}^{\text{am}}$ as well as the associated volume fractions. Rearrangement of (A.25) yields

$$\begin{aligned} \mathcal{C}^1 &= 2\eta_1 \mathcal{R}^1 \left[\left(\mathcal{C}^{\text{I}} \right)^{-1} - \eta_2 \left(\mathcal{C}^2 \right)^{-1} \mathcal{R}^2 \right]^{-1} \qquad \text{or} \\ \mathcal{C}^{\text{ip}} &= \left(1 - \eta_{\text{am}}\right) \mathcal{R}^{\text{ip}} \left[\left(\mathcal{C}^{\text{il}} \right)^{-1} - \eta_{\text{am}} \left(\mathcal{C}^{\text{am}} \right)^{-1} \mathcal{R}^{\text{am}} \right]^{-1} \end{aligned} \tag{A.26}$$

Similar treatment of Eq.(A.5) yields

$$\mathcal{C}^{\text{ip}} = \left[\mathcal{C}^{\text{il}} - \eta_{\text{am}} \mathcal{C}^{\text{am}} \mathcal{Q}^{\text{am}} \right] \left(\left(1 - \eta_{\text{am}}\right) \mathcal{Q}^{\text{ip}} \right)^{-1} \tag{A.27}$$

Obviously, Eqs.(A.26) and (A.27) have the familiar form of

$$\mathcal{X} = \mathcal{f}\left(\mathcal{X}\right) \tag{A.28}$$

where $\mathcal{f}$ is a non-linear tensorial function of $\mathcal{X}$. Apart from the arguments around the existence and uniqueness of the solution for Eq.(A.26) or (A.27), which are beyond the scope of this survey, the very first solution method which looks to suit the equation at hand is the numerical recursive method. In other words, some initial $\mathcal{C}^{\text{ip}}\Big|_{\text{initial}}$ is inserted into the right hand side of Eq.(A.26) or (A.27) whose result is fed into itself as many times as required until a certain convergence criterion is satisfied. For the problem examined in this study, it was observed that when $\mathcal{C}^{\text{il}}$ is of orthotropic symmetry, Eq.(A.28) converges to the solution using the recursive method while convergence problems is very likely when $\mathcal{C}^{\text{il}}$ has monoclinic symmetry. In the latter case, optimization techniques are certain alternatives although they may entail high computational cost.

Appendix B

Sensitivity/uncertainty analyses

To examine the sensitivity of the non-positive definiteness of the calculated $\mathcal{C}^{\mathrm{ip}}$ within $350\,\mathrm{K} < T < 400\,\mathrm{K}$, to the uncertainties available in $\mathcal{C}^{\mathrm{il}}$ and $\mathcal{C}^{\mathrm{am}}$, the following Monte Carlo sensitivity analysis has been performed. First, the following uncertainty intervals were considered for the amorphous Poisson's ratio, υ_{am}, and the amorphous Young's modulus, E_{am}, for the temperature range of 350K-400K.

$$\begin{aligned} &0.49 < \upsilon_{\mathrm{am}} < 0.49999 \\ &2\,\mathrm{MPa} < E_{\mathrm{am}} < 11.4\,\mathrm{MPa} \end{aligned} \tag{B.1}$$

Then in a total of 10^9 Monte Carlo cycles, at random temperatures, random E_{am} and υ_{am} are sampled from their assigned uncertainty intervals. Accordingly, a random $\mathcal{C}^{\mathrm{am}}$ is picked from its uncertainty space. Afterwards, at the same random temperature, a random $\mathcal{C}^{\mathrm{il}}$ is picked from its uncertainty space based on the uncertainty intervals obtained from the MC molecular simulations, except for C_{44}^{il} which is picked from $(82,100]$. Finally, using the DIM dissociation relationship, the new $\mathcal{C}^{\mathrm{ip}}$ and its eigenvalues are calculated. By carrying out this sensitivity analysis, none of the calculated interphase stiffnesses fulfilled the condition of positive definiteness. Given the extremely large number of the Monte Carlo cycles, it is very unlikely that one can find some temperature from $350\,\mathrm{K} < T < 400\,\mathrm{K}$ and some $\mathcal{C}^{\mathrm{am}}$ and $\mathcal{C}^{\mathrm{il}}$, as explained above, that can produce a positive definite $\mathcal{C}^{\mathrm{ip}}$. Therefore, one can conclude, with a high degree of certainty, that the non-positive definiteness of $\mathcal{C}^{\mathrm{ip}}$ within $350\,\mathrm{K} < T < 400\,\mathrm{K}$ is an established fact and insensitive to the uncertainties of $\mathcal{C}^{\mathrm{am}}$ and $\mathcal{C}^{\mathrm{il}}$.

Furthermore, the uncertainty intervals of $\mathcal{C}^{\mathrm{ip}}$ components originated from the uncertainties of $\mathcal{C}^{\mathrm{il}}$ components are calculated via the same Monte Carlo procedure: at a given temperature, the uncertainty space of $\mathcal{C}^{\mathrm{il}}$ is randomly sampled, $\mathcal{C}^{\mathrm{ip}}$s associated with each temperature are calculated, and finally the bounds of each component of $\mathcal{C}^{\mathrm{ip}}$ at each temperature are obtained (see Figs. B.1-B.3). Of the tensile components of $\mathcal{C}^{\mathrm{ip}}$, C_{33}^{ip} is the less sensitive and C_{11}^{ip} is the most sensitive component. Additionally, the non-orthotropic elements of $\mathcal{C}^{\mathrm{ip}}$ take small values close zero and exhibit a weak dependence on temperature.

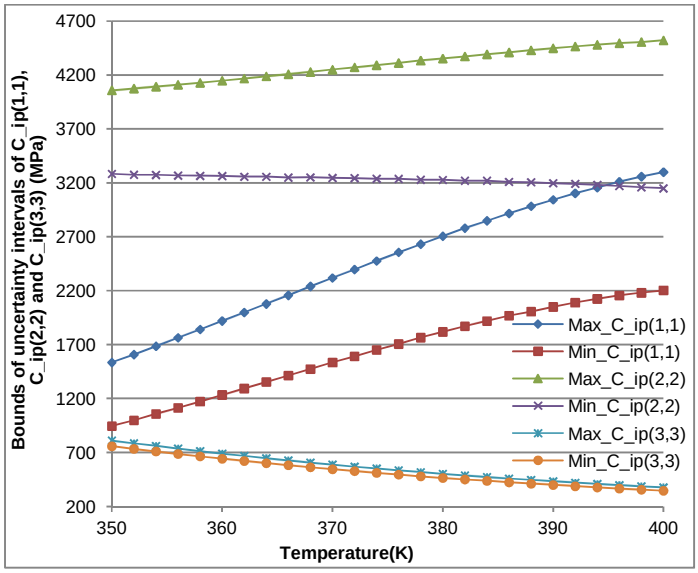

Fig. B.1 (color figure) Uncertainty intervals of normal components of $\mathcal{C}^{\mathrm{ip}}$ vs. temperature.

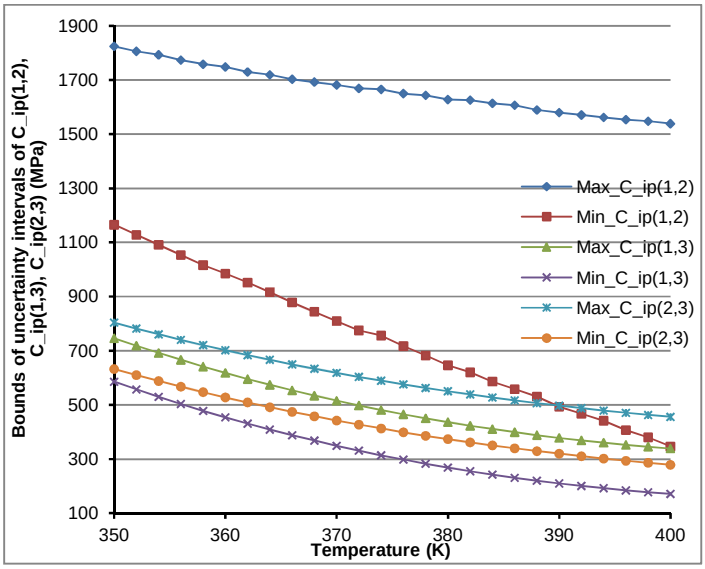

Fig. B.2 (color figure) Uncertainty intervals of C_{12}^{ip}, C_{13}^{ip} and C_{23}^{ip} vs. temperature.

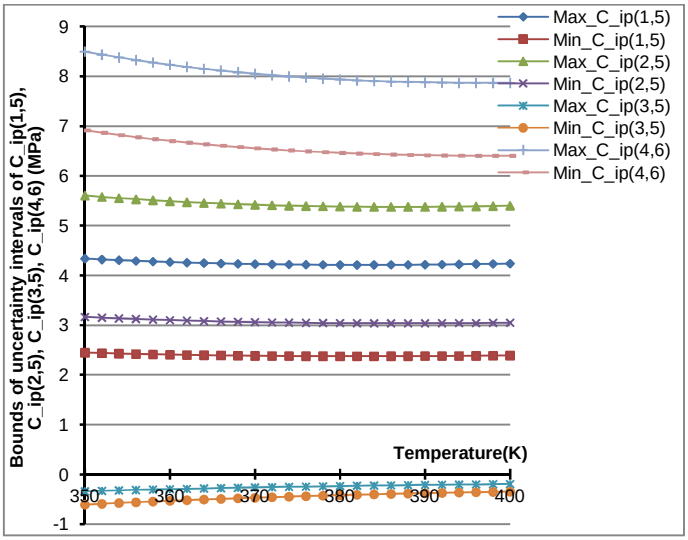

Fig. B3 (color figure) Uncertainty intervals of non-orthotropic elements C_{15}^{ip}, C_{25}^{ip}, C_{35}^{ip} and C_{46}^{ip} vs. temperature.

As an insightful examination, let us see what happens to the homogenized $\mathcal{C}^{il}$ if the components of $\mathcal{C}^{ip}$ beyond orthotropic symmetry are neglected. The omission of these elements may look reasonable as their absolute values are at least two orders of magnitude lower than the other elements of $\mathcal{C}^{ip}$, except for the negative shearing stiffnesses. As reflected in Table B1, the newly homogenized $\mathcal{C}^{il}$ is once calculated with a $\mathcal{C}^{ip}$ of orthotropic symmetry and again with an orthotropic $\mathcal{C}^{ip}$ excluding the small negative shearing stiffnesses C_{44}^{ip} and C_{55}^{ip}. The tensile components of the two newly calculated effective $\mathcal{C}^{il}$s are identical and close to their corresponding components in the initial $\mathcal{C}^{il}$ appearing in Table 1. On the other hand, the non-orthotropic components of $\mathcal{C}^{ip}$ have no impact on C_{44}^{il}, a weak impact on C_{55}^{il} and a strong impact on C_{66}^{il}, which may be viewed as another evidence for the dissimilarity between C_{66}^{ip} and the two other shearing components of $\mathcal{C}^{ip}$. It is clearly seen that although the small negative shearing stiffnesses C_{44}^{ip} and C_{55}^{ip} may look negligible and unimportant at first glance, they can produce corresponding C_{44}^{il} and C_{55}^{il} that are two to three orders greater in magnitude.

As a last sensitivity check, only the orthotropic part of $\mathcal{C}^{il}$ has been preserved and the dissociation analysis at the same temperature of 370 K was carried out. Table B2 confirms that $\mathcal{C}^{ip}$s calculated using the two approaches match perfectly. The tensile elements of the newly calculated $\mathcal{C}^{ip}$ are still close to their corresponding components of $\mathcal{C}^{ip}$, given in Table 1 and calculated using a $\mathcal{C}^{il}$ of monoclinic symmetry. Contrary to the situation reflected in Table 1, here the ECIM converges to the same solution output by the DIM using the numerical recursive method. Indeed, a combination of dual formulae (6) was used to achieve the convergence. More interestingly, it is observed that the controversial shearing stiffnesses C_{44}^{ip} and C_{55}^{ip} appearing in Table B2 are equal to those appearing in Table 1, suggesting that these two shearing stiffnesses

are very robust to or, more precisely, independent of the non-orthotropic components of $\mathcal{C}^{\mathrm{il}}$. The last shearing stiffness, C_{66}^{ip}, however, exhibits a strong dependence on non-orthotropic components; another dissimilarity which might have been expected in advance.

Table B1: The effect of negligible terms of $\mathcal{C}^{\mathrm{ip}}$ on the homogenized $\mathcal{C}^{\mathrm{il}}$

at T=370 K: $E_{\mathrm{am}}=6.31\mathrm{MPa}$, $G_{\mathrm{am}}=2.1\mathrm{MPa}$, $\eta_{\mathrm{am}}=0.66$, $\eta_{\mathrm{ip}}=0.34$												
$\mathcal{C}^{\mathrm{ip}}\,(\mathrm{MPa})$ (Taken from Table 1 after eliminating nonzero terms beyond orthotropic symmetry)							$\mathcal{C}^{\mathrm{il}}\,(\mathrm{MPa})$					
1972.2	1307.4	427.7	0	0	0	$\Rightarrow$	1600.5	1414.3	1134.4	0	0	0
1307.4	3824.3	524.2	0	0	0		1414.3	2304.6	1205.3	0	0	0
427.7	524.2	567.3	0	0	0		1134.4	1205.3	1238.1	0	0	0
0	0	0	**-1.11**	0	0		0	0	0	90	0	0
0	0	0	0	**-1.08**	0		0	0	0	0	220.7	0
0	0	0	0	0	320.5		0	0	0	0	0	109.3
$\mathcal{C}^{\mathrm{ip}}\,(\mathrm{MPa})$ (Taken from Table 1 after eliminating small negligible elements)							$\mathcal{C}^{\mathrm{il}}\,(\mathrm{MPa})$					
1972.2	1307.4	427.7	0	0	0	$\Rightarrow$	1600.5	1414.3	1134.4	0	0	0
1307.4	3824.3	524.2	0	0	0		1414.3	2304.6	1205.3	0	0	0
427.7	524.2	567.3	0	0	0		1134.4	1205.3	1238.1	0	0	0
0	0	0	0	0	0		0	0	0	0	0	0
0	0	0	0	0	0		0	0	0	0	0	0
0	0	0	0	0	320.5		0	0	0	0	0	109.3

Table B2: Impact of nonorthotropic components of $\mathcal{C}^{\mathrm{il}}$ on the dissociated $\mathcal{C}^{\mathrm{ip}}$

at T=370 K: $E_{\mathrm{am}}=6.31\mathrm{MPa}$, $G_{\mathrm{am}}=2.1\mathrm{MPa}$, $\eta_{\mathrm{am}}=0.66$, $\eta_{\mathrm{ip}}=0.34$												
$\mathcal{C}^{\mathrm{am}}\,(\mathrm{MPa})$							$\mathcal{C}^{\mathrm{il}}$ (taken from [20] after eliminating nonorthotropic elements)					
3097.9	3093.7	3093.7	0	0	0		1749.9	1613.6	1092.9	0	0	0
3093.7	3097.9	3093.7	0	0	0		1613.6	2569.3	1150	0	0	0
3093.7	3093.7	3097.9	0	0	0		1092.9	1150	1249.6	0	0	0
0	0	0	2.1	0	0		0	0	0	90	0	0
0	0	0	0	2.1	0		0	0	0	0	220	0
0	0	0	0	0	2.1		0	0	0	0	0	570
Then:												
$\mathcal{C}^{\mathrm{ip}}\,(\mathrm{MPa})$ output by the DIM			2569.8	2074.1	362.03	0	0	0				
			2074.1	4807.8	439.96	0	0	0				
			362.03	439.96	574.47	0	0	0				
			0	0	0	**-1.11**	0	0				
			0	0	0	0	**-1.08**	0				
			0	0	0	0	0	1688.6				
$\mathcal{C}^{\mathrm{ip}}\,(\mathrm{MPa})$ output by the ECIM using numerical recursive method			2569.8	2074.1	362.03	0	0	0				
			2074.1	4807.8	439.96	0	0	0				
			362.03	439.96	574.47	0	0	0				
			0	0	0	**-1.11**	0	0				
			0	0	0	0	**-1.08**	0				
			0	0	0	0	0	1688.6				

References

1. M. Hütter; P. J. in 't Veld; G. C. Rutledge. *Polymer* **2006,** 47, 5494-5504.
2. L. Lin; A. S. Argon. *J. Mater. Sci.* **1994,** 29, 294-323.
3. G. Coulon; G. Castelein; C. G'Sell. *Polymer* **1999,** 40, 95-110.
4. X. Guan; R. Pitchumani. *Polym. Eng. Sci.* **2004,** 44, 433-451.
5. A. Odajima; T. Maeda. *Journal of Polymer Science Part C: Polymer Symposia* **1967,** 15, 55-74.
6. J. Janzen. *Polym. Eng. Sci.* **1992,** 32, 1255-1260.
7. R. H. Boyd. *Journal of Polymer Science: Polymer Physics Edition* **1983,** 21, 493-504.
8. D. J. Lacks; G. C. Rutledge. *J. Phys. Chem.* **1994,** 98, 1222-1231.
9. G. C. Rutledge. In Simulation Methods for Polymers; M. Kotelyanskii; D. N. Theodorou, Eds.; Marcel Dekker Inc.: New York, 2004, pp 359-388.
10. M. M. Zehnder; A. A. Gusev; U. W. Suter. *Revue de l'Institute Francais du Petrole* **1996,** 51, 131-137.
11. A. Singhal; L. J. Fina. *Polymer* **1996,** 37, 2335-2343.
12. S. Balijepalli; G. C. Rutledge. *J. Chem. Phys.* **1998,** 109, 6523-6526.
13. J. Menczel; B. Wunderlich. *Journal of Polymer Science: Polymer Letters Edition* **1981,** 19, 261-264.
14. P. J. Flory. *J. Am. Chem. Soc.* **1962,** 84, 2857-2867.
15. A. Sedighiamiri; T. B. Van Erp; G. W. M. Peters; L. E. Govaert; J. A. W. Van Dommelen. *J. Polym. Sci., Part B: Polym. Phys.* **2010,** 48, 2173-2184.
16. O. Gueguen; S. Ahzi; A. Makradi; S. Belouettar. *Mechanics of Materials* **2010,** 42, 1-10.
17. R. M. Christensen; K. H. Lo. *Journal of the Mechanics and Physics of Solids* **1979,** 27, 315-330.
18. C. C. Kiritsi; N. K. Anifantis. *Computational Materials Science* **2001,** 20, 86-97.
19. B. Zhang; B. Gu. 2011, p 303-307.
20. P. J. in ‘t Veld; M. Hütter; G. C. Rutledge. *Macromolecules* **2006,** 39, 439-447.
21. B. Crist; C. J. Fisher; P. R. Howard. *Macromolecules* **1989,** 22, 1709-1718.
22. T. M. Krigas; J. M. Carella; M. J. Struglinski; B. Crist; W. W. Graessley; F. C. Schilling. *Journal of polymer science. Part A-2, Polymer physics* **1985,** 23, 509-520.
23. K. H. Hellwege; W. Knappe; P. Lehmann. *Kolloid-Zeitschrift & Zeitschrift für Polymere* **1962,** 183, 110-120.
24. J. Janzen. *Polym. Eng. Sci.* **1992,** 32, 1242-1254.
25. F. Bédoui; J. Diani; G. Régnier; W. Seiler. *Acta Mater.* **2006,** 54, 1513-1523.
26. L. J. Fetters; D. J. Lohse; D. Richter; T. A. Witten; A. Zirkel. *Macromolecules* **1994,** 27, 4639-4647.
27. S. Humbert; O. Lame; R. Séguéla; G. Vigier. *Polymer* **2011,** 52, 4899-4909.
28. P. Anil Kumar; R. K. Gupta. Fundamentals Of Polymer Engineering (power Engineering, 66); Marcel Dekker, 2003.
29. S. Nikolov; I. Doghri. *Polymer* **2000,** 41, 1883-1891.
30. M. Hori; S. Nemat-Nasser. *Mechanics of Materials* **1993,** 14, 189-206.
31. S. Ahzi; D. M. Parks; A. S. Argon. 1995, pp 31-40.
32. S. Ahzi; N. Bahlouli; A. Makradi; S. Belouettar. *Journal of Mechanics of Materials and Structures* **2007,** 2, 1-22.
33. K. Yoshimoto; T. S. Jain; K. V. Workum; P. F. Nealey; J. J. de Pablo. *Phys. Rev. Lett.* **2004,** 93, 175501.
34. R. S. Lakes; W. J. Drugan. *Journal of the Mechanics and Physics of Solids* **2002,** 50, 979-1009.
35. D. M. Kochmann; W. J. Drugan. *Journal of the Mechanics and Physics of Solids* **2009,** 57, 1122-1138.
36. H. H. Huang; C. T. Sun. *Journal of the Mechanics and Physics of Solids* **2011,** 59, 2070-2081.
37. R. S. Lakes; T. Lee; A. Bersie; Y. C. Wang. *Nature* **2001,** 410, 565-567.
38. T. Jaglinski; D. Kochmann; D. Stone; R. S. Lakes. *Science* **2007,** 315, 620-622.
39. D. Y. Yoon; P. J. Flory. *Macromolecules* **1984,** 17, 868-871.

40. W. A. Counts; M. Friák; C. C. Battaile; D. Raabe; J. Neugebauer. *physica status solidi (b)* **2008,** 245, 2630-2635.
41. R. Hill. *Proceedings of the Physical Society. Section A* **1952,** 65, 349-354.
42. L. Ding; R. L. Davidchack; J. Pan. *Journal of the Mechanical Behavior of Biomedical Materials* **2012,** 5, 224-230.